Earth and Planetary Science Letters, 111 (1992) 241–255
Elsevier Science Publishers B.V., Amsterdam

[CL]

Element partitioning between silicate minerals and coexisting melts at pressures of 1–27 GPa, and implications for mantle evolution

Reidar G. Trønnes [a], Dante Canil [b] and Kejian Wei [a]

[a] *C.M. Scarfe Laboratory of Experimental Petrology, Department of Geology, University of Alberta, Edmonton, Alta T6G 2E3, Canada*
[b] *Bayerisches Geoinstitut, Universität Bayreuth, D-8580 Bayreuth, Germany*

Received September 3, 1991; revision accepted April 15, 1992

ABSTRACT

Major element partitioning data relevant to melt generation and separation at various depths in the mantle have been derived from the compositions of coexisting silicate minerals and quenched melts in our melting experiments on komatiites and C1 chondrite at 4–11 GPa and 20–27 GPa respectively, and from published experimental studies covering the 1–26 GPa range. In these experiments there is a general positive correlation between pressure, temperature and the normative olivine content of the melts. The $K_D^{Si/Mg}$(mineral/melt) for olivine/β-spinel, pyroxenes, and garnet/majorite increases markedly with increasing depth, especially in the 30–180 km range, and exceeds unity for majorite and perovskite. The $K_D^{Fe/Mg}$ remains well below unity throughout the entire depth (pressure and temperature) range for all of the minerals (0.3–0.5 for β-spinel, majorite and perovskite). The $K_D^{Ca/Al}$ for garnet/majorite remains low (0.1–0.3), decreases with increasing depth for olivine/β-spinel ($\leqslant 1$ at pressures exceeding 10 GPa), and remains near unity for the pyroxenes. The Nernst mineral/melt distribution coefficient for Cr (D_{Cr}) decreases with increasing depth for all minerals. Whereas garnet/majorite D_{Cr} remains above 1, the values for the pyroxenes and olivine/β-spinel are nearly constant at 0.3–0.5 in the 10–20 GPa range. All the distribution coefficients derived for perovskite overlap those of majorite.

These partitioning relationships indicate that the ratio Mg/(Mg + Fe) of upper mantle peridotites is a largely depth-independent measure of the degree of melt depletion. Because the bulk $K_D^{Ca/Al}$ for assemblages containing garnet/majorite is below unity at depths exceeding 150 km, melt separation will lead to a decreased Ca/Al ratio in residues and correspondingly Al-depleted magmas. Al-undepleted komatiites must form by melt separation from harzburgitic or dunitic residues following extensive melting. The higher than chondritic Ca/Al ratio of sampled upper mantle peridotites may result from minor fractionation of majorite and perovskite in combination with the addition of some Al-depleted komatiitic magma to the uppermost mantle.

The bulk residue D_{Cr} decreases with increasing depth of melting, and garnet/majorite-bearing residues will have D_{Cr} near unity at depths exceeding 150 km. Extensive melting and melt extraction from garnet/majorite-free residues at such depths will lead to a bulk D_{Cr} of 0.3–0.5. The chemistry of variably depleted mantle peridotites points to a bulk D_{Cr} of about 1 during the melt extraction, indicating that a major part of the time-integrated melt extraction occurred in the deeper parts of the upper mantle. Much of the melt depletion occurred in the form of early komatiitic magmatism but high-MgO primary magma extraction followed by shallow-level fractionation may have also been important in recent geological time.

1. Introduction

Recent quantitative modelling of planetary accretion processes has provided strong evidence for a partially or totally molten Earth in its early evolutionary stage [e.g. 1]. Later partial melting and melt extraction from the mantle to produce oceanic and continental crust has further modified the mantle, although the oceanic lithosphere is recycled back into the mantle by subduction. Melt-solid fractionation processes therefore play a fundamental role in the chemical evolution of the Earth's mantle, regardless of whether or not a Hadean mantle-wide magma ocean existed. The chemical consequences of partial melt extraction

Correspondence to: R.G. Trønnes, Geological Survey of Norway, P.O. Box 3006, Lade, N-7002 Trondheim, Norway.

TABLE 1

Chemical composition of quenched liquids and coexisting minerals

No.	SiO_2	Al_2O_3	Cr_2O_3	FeO	MgO	CaO	Total							
AUK:	45.6	7.95	0.29	12.7	25.0	7.60	97.8							
Quenched liquids								T (°C)	p (GPa)	t (min)	Liquidus mineral			
202	45.8	9.62	0.41	12.8	21.4	9.62	99.7	1650	4.0	65	olivine			
135	46.3	8.45	0.40	13.1	21.6	9.17	99.0	1770	5.0	5	olivine			
260	47.4	5.91	0.55	10.9	28.1	5.99	98.9	1780	5.5	5	olivine			
569	40.9	6.01	0.34	14.4	24.3	8.18	94.1	1800	5.7	5	garnet			
168U	46.3	7.40	0.48	11.2	25.0	7.95	98.3	1800	6.0	10	garnet			
1272 **	43.2	4.70	0.20	15.6	23.2	10.8	97.7	1870 *	8.5	10	garnet			
Olivine								Si	Al^{IV}	Al^{VI}	Cr	Fe	Mg	Ca
202	40.2	0.22	0.20	10.3	47.5	0.34	98.8	1.000	–	0.006	0.004	0.214	1.761	0.009
135	40.0	0.21	0.18	10.5	47.7	0.33	98.9	0.995	0.005	0.001	0.003	0.218	1.769	0.009
260	40.6	0.19	0.18	6.65	50.6	0.20	98.4	0.997	0.003	0.002	0.003	0.137	1.852	0.005
Garnet								Si^{IV}	Si^{VI}	Al	Cr	Fe	Mg	Ca
569	44.0	21.7	1.15	5.85	23.2	4.01	99.9	3.000	0.080	1.790	0.061	0.342	2.421	0.301
168U	44.2	21.0	1.16	5.10	25.0	3.61	100.1	3.000	0.080	1.724	0.061	0.297	2.596	0.269
1272	44.3	20.3	0.80	5.74	23.2	5.31	99.7	3.000	0.123	1.687	0.042	0.322	2.438	0.401
Pyroxene							Si	Al^{IV}	Al^{VI}	Cr	Fe	Mg	Ca	
135	55.9	3.13	0.45	6.26	31.9	2.40	100.0	1.937	0.063	0.065	0.012	0.181	1.647	0.089
569	54.8	1.85	0.26	6.21	33.3	2.38	98.8	1.928	0.072	0.005	0.007	0.183	1.746	0.090
	54.0	2.54	0.21	6.42	27.1	8.05	98.3	1.939	0.061	0.046	0.006	0.193	1.450	0.310
ADK:	46.8	3.42	0.34	11.1	31.5	5.67	98.8							
Quenched liquids								T (°C)	p (GPa)	t (min)	Liquidus mineral			
138	44.4	3.57	0.34	12.1	28.0	7.47	95.9	1700	4.0	5	olivine			
236	48.3	4.04	0.42	11.4	27.6	7.12	98.9	1750	5.0	10	olivine			
168D	48.4	3.27	0.33	11.2	29.7	5.80	98.7	1800	6.0	10	olivine			
156	45.1	3.51	0.29	11.6	27.8	7.26	95.6	1830	7.0	7	olivine			
1328	46.5	4.29	0.35	11.4	28.7	7.95	99.2	1900 *	8.0	8	olivine			
1276 **	46.1	4.65	0.34	13.5	25.6	7.72	97.9	1910 *	8.5	15	olivine			
1236	46.8	3.77	0.34	10.8	31.2	5.25	98.2	1920 *	9.5	20	olivine			
1330	45.8	3.49	0.32	11.7	29.2	7.90	98.4	1930 *	10.0	10	olivine			
1242	46.5	3.83	0.33	10.4	31.3	6.27	98.6	1940 *	10.5	60	olivine			
DC409 #	46.8	3.42	0.34	11.1	31.5	5.67	98.8	1950 *	11.0	5	garnet			
Olivine								Si	Al^{IV}	Al^{VI}	Cr	Fe	Mg	Ca
138	40.2	0.15	0.13	8.74	50.1	0.22	99.5	0.986	0.004	–	0.002	0.179	1.832	0.006
236	41.3	–	0.15	8.60	49.8	0.23	100.1	1.005	–	–	0.003	0.175	1.806	0.006
168D	41.5	–	0.10	7.00	50.3	0.20	99.1	1.011	–	–	0.002	0.143	1.827	0.005
156	41.5	–	0.15	7.40	50.9	0.23	100.2	1.003	–	–	0.003	0.150	1.834	0.006
1328	41.3	0.23	0.11	7.15	50.9	0.31	100.0	0.999	0.001	0.006	0.002	0.145	1.836	0.008
1276	40.8	0.21	0.11	8.77	49.6	0.23	99.7	0.998	0.002	0.004	0.002	0.179	1.808	0.006
1236	41.2	0.21	0.10	6.04	52.5	0.19	100.2	0.990	0.006	–	0.002	0.121	1.881	0.005
1330	41.0	0.23	0.09	6.55	51.6	0.27	99.7	0.993	0.007	–	0.002	0.145	1.836	0.008
1242	41.2	0.23	0.11	6.07	52.2	0.26	100.1	0.992	0.007	–	0.002	0.122	1.874	0.007
Garnet								Si^{IV}	Si^{VI}	Al	Cr	Fe	Mg	Ca
DC409	47.7	15.1	1.12	5.30	20.0	2.64	99.8	3.000	0.321	1.239	0.059	0.309	2.906	0.197
Pyroxene								Si	Al^{IV}	Al^{VI}	Cr	Fe	Mg	Ca
138	56.2	1.47	0.23	4.79	34.0	2.09	98.8	1.958	0.042	0.018	0.006	0.140	1.766	0.078
1328	57.3	1.73	0.17	4.51	34.2	2.30	100.2	1.964	0.036	0.034	0.004	0.129	1.747	0.084
DC409	58.7	0.38	0.11	3.32	36.0	0.64	99.2	2.009	–	0.015	0.003	0.095	1.836	0.023

or fractional crystallization are goverened by the partitioning of the various elements between the coexisting minerals and melts.

In particular, the Fe/Mg partitioning between olivine and basaltic melt at pressures below 3 GPa [2–4] has been an extremely useful guide to the degree of melt depletion in residual peridotites and is commonly used to estimate the compositions of source regions for mafic volcanics. Compositional data on coexisting phases in products of recent melting experiments have led some authors to either assume or conclude that the direction and magnitude of the Fe/Mg mineral–melt partitioning is similar in the deeper portions of the upper mantle [e.g. 5,6]. In contrast, the values of the coefficient $K_D^{Fe/Mg} = (Fe/Mg)^{min}/(Fe/Mg)^{melt}$ extrapolated from the 1–3 GPa range [3,4] to the 13–15 GPa range approach unity.

Although less regular than the olivine-liquid Fe/Mg partitioning at low pressure, the partitioning of other major and minor elements (e.g. Ca, Al and Cr) between mantle minerals and coexisting melts may provide an insight into the processes associated with basaltic to komatiitic magmatism and differentiation of the Earth. Important issues to be adressed include the origin of the small, but significant, deviation of the Ca/Al ratio in upper mantle peridotites from the chondritic ratio [7], and the indication from (residual) mantle peridotites that the bulk mineral-melt partitioning coefficient for Cr was close to unity [8]. During melting and melt extraction at pressures below 3 GPa the bulk mineral melt partitioning coefficient for Cr is probably considerably greater than unity [9].

Much of the melt extraction and melt-solid fractionation modifying the composition of the upper mantle occurs at depths exceeding 90 km [5,8,10–12]. Experimentally derived element partitioning data at pressures above 3 GPa are therefore required for a complete understanding of the processes responsible for this differentiation. In this paper, we report on the compositions of coexisting liquidus and near-liquidus minerals and the coexisting quenched melts from our melting experiments on two komatiites at pressures of 4–11 GPa [13] and average C1 chondrite at 20–27 GPa [14]. The mineral-melt partitioning coefficients derived from the coexisting phase compositions, combined with corresponding data derived from published experimental studies on peridotitic and chondritic compositions in the 5–26 GPa range, and on basaltic and peridotitic compositions in the 1–4 GPa range, are then used as constraints on the magmatic processes leading to the present composition of upper mantle peridotites.

2. Experimental and analytical methods

The starting materials and experimental methods are described in [13] and [14]. We now suspect that the calibration curve of Wei et al. [13] used for pressures above 9 GPa was markedly biased towards higher sample pressures. To further investigate the phase relationships of the Al-depleted komatiite (ADK) near the olivine–garnet cosaturation point, we performed additional multi-anvil experiments [1236, 1242, 1276, DC409 as well as 1272 (AUK); see Table 1] using a 14 mm octahedral pressure cell, 8 mm anvil

Notes to Table 1:

Starting compositions: AUK = Al-undepleted komatiite (sample M620); ADK = Al-depleted komatiite (sample HSS-15). Oxide abundances are in weight percent. Mineral formula units are normalized to 4, 12 and 6 oxygen atoms for olivine, garnet and pyroxene, respectively. The reported analyses represent averages of 3–12 (mostly 5) spot analyses. The average precison (1σ) of the quenched liquid analyses is 2% for SiO_2 and CaO, 3% for Al_2O_3 and MgO, 5% for FeO, and 11% for Cr_2O_3. For the mineral analyses the precision is generally better than 1% for oxides with total abundances of 30–50%, better than 3% for oxides at the 5–30% abundance level, and better than 8% for the minor and trace oxides, except for Cr_2O_3. The precision of the Cr_2O_3 analyses of minerals is generally better than 10% when the total abundance is about 1% (garnet) and 30% when the abundance is below 0.5%. Based on repeated analyses of standards the analytical accuracy is estimated to be similar to the precision.

* Estimated liquidus temperature.

** Experiment 'reversed' by first increasing the temperature to 50°C above the run condition, followed by slow temperature decrease to the run condition. The large differences between these melt compositions and the starting compositions are caused by the presence of relatively large amounts of a single liquidus phase (garnet in 1272 and olivine in 1276).

\# Not analyzed, but assumed equal to bulk system composition because of low proportion of minerals present (see Fig. 3).

truncations (14–8 mm configuration), $LaCrO_3$-heaters, Re capsules, and WRe thermocouples inserted axially through sintered alumina rods isolated from the heaters by magnesia sleeves. Whereas the highest pressure calibration point in the 18–11 mm configuration of [13] was the coesite–stishovite transition at 9.1 GPa and 1000°C, the 14–8 mm configuration was calibrated at 1000 and 1600°C up to the olivine-modified spinel transition at 13.7 GPa and 15.1 GPa respectively. The new experiments appear to confirm the suspected sample pressure bias above 9 GPa. We do not include the mineral-melt partitioning results from the highest pressure experiments (> 9 GPa) of [13] in this paper but prescribe the following approximate pressure correction: pressures reported in [13] as 12, 11 and 10 GPa should be 10.5, 10 and 9.5 GPa, respectively.

Wei et al. [13] used sample capsules of graphite and molybdenum, but no metallic Fe or Fe-Mo alloy was observed in the run products. This is in contrast to the somewhat higher pressure experiments of Herzberg [15] (16 GPa) and Takahashi [16] (10–14 GPa). We detected small amounts of Mo in the quenched liquid portion of the run products from the Mo capsules, but no Fe loss to either the Mo, C or Re capsules in any of the komatiite experiments. Small Re fragments surrounded by quenched melt in the 20–27 GPa C1 chondrite experiments [14] contain up to 2–5 wt% FeO, but Fe loss cannot be detected by analyses of the quenched melt. The run durations, ranging from 5 to 65 minutes, are listed in Table 1 and Table 2. Two of the experiments (AUK:1272 and ADK:1276) were 'reversed' by first increasing the temperature to 50°C above the run temperature prior to slow cooling towards the run temperature.

The liquidus minerals and coexisting quench crystallized melts were analyzed with a Cameca Camebax SX50 instrument at the *Bayerisches Geoinstitut* and an ARL-SEMQ instrument at the University of Alberta, using the wavelength dispersive mode, accelerating voltage of 15 kV, probe current of 12–15 nA measured on brass, counting time of 20 s on peaks, and a selection of natural mineral standards. The quenched melts were analyzed with a defocussed beam of about 30 μm in diameter (700 μm^2) at the *Bayerisches Geoinstitut* and by a raster mode of analysis covering areas of 400 μm^2 at the University of Alberta. Although the compositional variations within the quenched melt portion of the run products are not significantly greater than the analytical precision (see Table 1), regions close to the liquidus were selected for analysis. The mineral analyses were performed on grains at or near the liquidus. The compositional variation within and between these grains does not exceed the analytical precision (Table 1). The composition of some of the phases, especially garnet and majorite, changes dramatically as a function of the distance (and therefore temperature difference) from the liquidus [see 14,15].

TABLE 2

Majorites and perovskite at or near the liquidus in experiments on a model C1-chondritic composition in the CMFAS system

No.	SiO_2	Al_2O_3	FeO	MgO	CaO	Total			
Bulk system	34.2	2.47	36.8	24.6	1.95	100.0			
Majorite							Liq. T (°C)	p (GPa)	t (min)
1245	47.6	14.5	10.5	25.5	2.10	100.2	2030	20	15
1251	47.8	13.1	10.3	26.4	1.94	99.3	2120	23	30
1273	48.2	11.3	11.3	26.1	2.80	99.7	2150	25 (+0.3/−0.6)	12
1274	48.0	13.0	11.2	25.6	2.50	100.3	2170	27 (+0.6/−1.2)	10
Perovskite									
1274	50.4	5.64	13.5	29.6	0.63	99.8	2170	27 (+0.6/−1.2)	10

Oxide abundances are in weight percent. The reported analyses represent averages of 10–20 spot analyses. The average precision and accuracy values are comparable to those given in Table 1

3. Liquidus phase relations of peridotite, komatiite and chondrite

3.1 Peridotite phase relations to 27 GPa

As a basis for discussing bulk mineral-melt distribution coefficients during melting and fractionation in the upper mantle, the transition zone and the uppermost lower mantle, the changes in liquidus and solidus mineralogy as a function of pressure must be considered. In peridotitic mantle compositions the liquidus phase is olivine up to pressures of 13–15 GPa (cosaturation with majorite) [15–17]. Liquidus majorite persists to pressures of 24–26 GPa, and at higher pressures perovskite is the liquidus phase [17,18]. The exact locations of the olivine-majorite and majorite-perovskite cotectics in terms of pressure is compositionally dependent, with the more silica- and alumina-rich compositions (e.g. model mantle based with a chondritic Si/Mg ratio [18]) having the most extensive majorite liquidus fields. With increasing pressure from 5 GPa until the disappearance of pyroxene at 14–15 GPa [19], the modal amount of subsolidus garnet increases in parallel with increased pyroxene dissolution in the garnet. A bimineralic subsolidus assemblage of majorite and β-spinel persists to about 22 GPa, where β-spinel breaks down to form perovskite and magnesiowüstite [20]. In experiments at 25 GPa on peridotitic and model chondritic mantle compositions, magnesiowüstite was recorded only below the solidus by Ito and Takahashi [17] and just above the solidus by Ohtani and Sawamoto [18].

3.2 Komatiite phase relations and the pyroxene problem

The phase relations of the Al-undepleted (AUK, sample M620) and the Al-depleted (ADK, sample HSS-15) komatiites were reported by Wei et al. [13], and the problem of distinguishing between separate high-Ca (5–12 wt% CaO) and

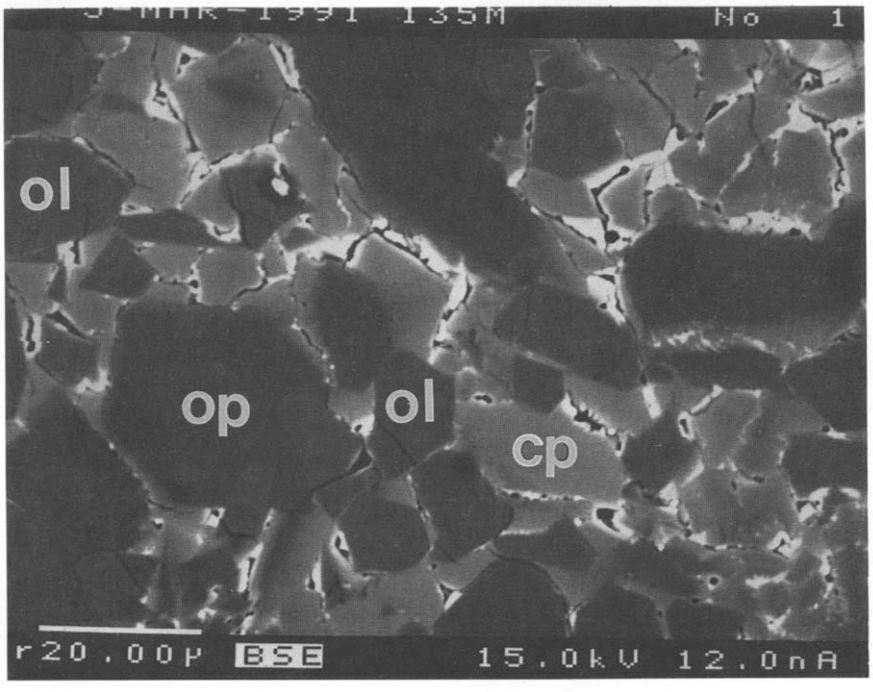

Fig. 1. SEM-BSE image of komatiite (AUK) run product from experiment 135 at 5 GPa (Table 1). The crystallization sequence is olivine (*ol*, intermediate brightness) followed by low-Ca pyroxene cores (*op*, lowest brightness) and high-Ca pyroxene overgrowths/quench clinopyroxene (*cp*, highest brightness). The width of the image is 0.1 mm.

low-Ca (2–6 wt% CaO) pyroxenes (referred to below as 'cpx' and 'opx', respectively) of high-temperature origin was discussed. Herzberg et al. [15] found that it was often impossible to distinguish between primary and quench cpx. The latter was found to contain up to 10 wt% Al_2O_3 and often occurs as elongate, but large and well-defined, grains perpendicular to the liquidus interphase. Based on their experiments in the CMAS system, Herzberg et al. [15] also demonstrated that the isobaric invariant points for komatiitic and peridotitic compositions at 5–10 GPa are peritectics rather than eutectics, and that the reaction is opx + liquid = cpx + olivine + garnet.

In spite of its elongate appearance and orientation perpendicular to the liquidus, Wei et al. [13] interpreted the liquidus pyroxene of the ADK composition in experiment 275 to be primary. This interpretation was mainly based on the reported Al_2O_3 content of 2.3%. A reexamination of the textures of this run product, using a higher quality back-scattered electron imaging system at the *Bayerisches Geoinstitut*, has revealed a more complex picture. Elongate and partly oriented cpx are present together with olivine along the liquidus. These cpx grains have a variable composition, with up to 5% Al_2O_3 and up to 11% CaO. In some places they also appear to form branching crystals, and we now interprete them as quench crystals. Quench cpx overgrowths on opx and olivine are also found in some of the experiments (Fig. 1).

The primary liquidus phases for the key experiments analyzed in this study are shown in Table 1. At low pressure the crystallization sequence is olivine (liquidus phase) followed by opx and then garnet. This crystallization sequence is reversed at pressures above the olivine-garnet cosaturation

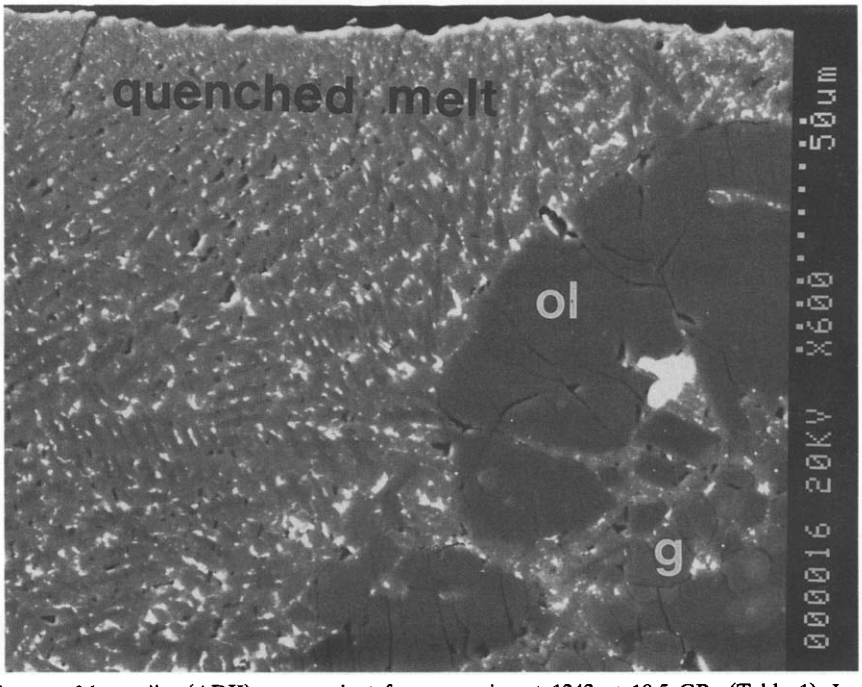

Fig. 2. SEM-BSE image of komatiite (ADK) run product from experiment 1242 at 10.5 GPa (Table 1). Large olivine crystals (darkest, *ol*) are found closest to the liquidus, and small, round garnet grains (lighter, *g*) are located further away from the liquidus. Small, light inclusions in the olivines are Ca-rich, Al-poor garnets of subsolidus composition [see 15]. The separate garnet grains also have a CaO/Al_2O_3 ratio (0.28–0.30) that is higher than that expected for true liquidus garnets (0.17 for the 9.5 and 11 GPa liquidus garnets, Table 1). A very bright Re fragment (capsule wall material) is present between the olivine and garnet crystals. The width of the image is 0.2 mm.

point (5–6 GPa for AUK and near 10.5 GPa for ADK). The liquidus phase relations just below and just above the olivine-garnet cosaturation point for the ADK are illustrated in Fig. 2 and Fig. 3. At 10.5 GPa (experiment 1242, Fig. 2) large olivine grains border the liquid part of the charge, whereas small round garnet crystals occur further away from the liquidus. At 11 GPa (ex-

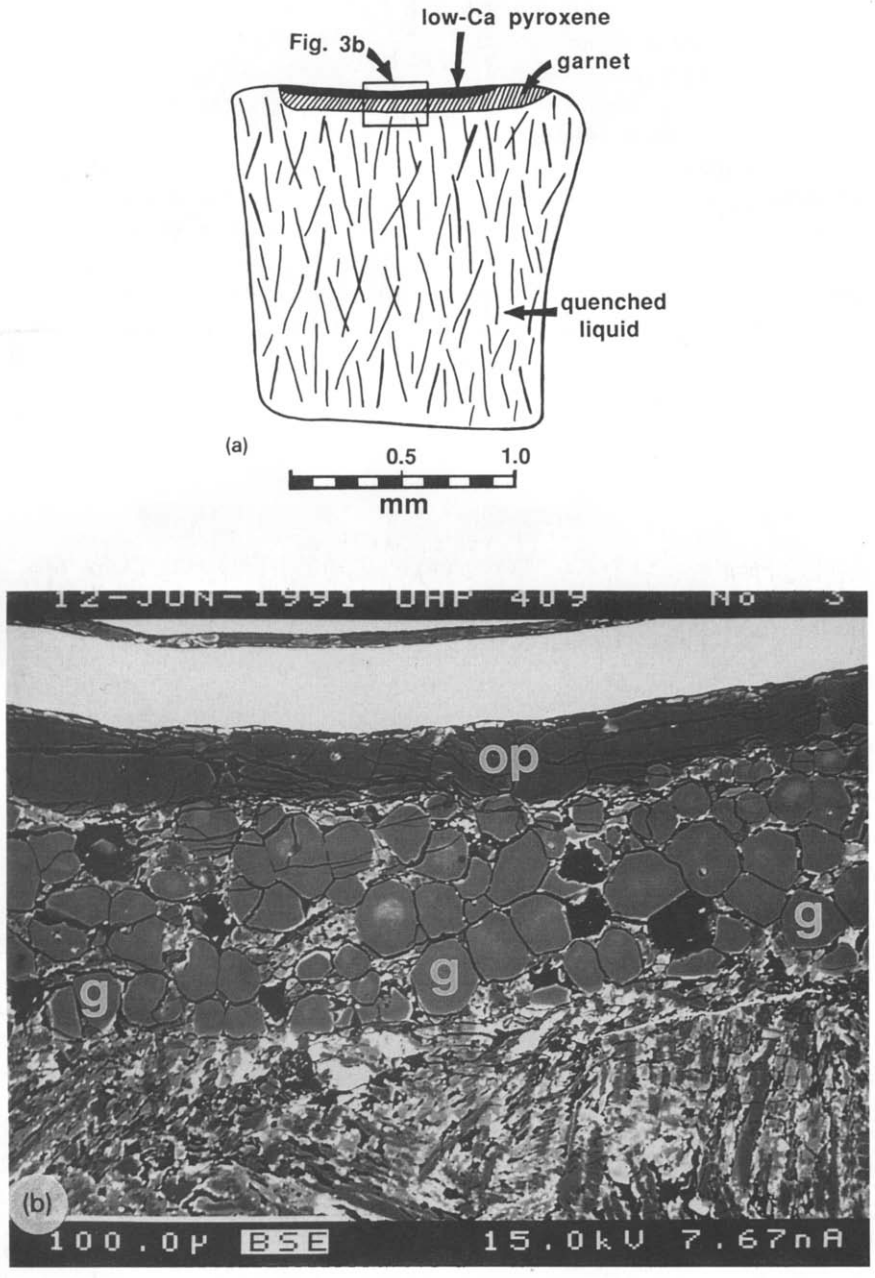

Fig. 3. (a) Sketch of komatiite (ADK) run product of experiment DC409 at 11 GPa (Table 1). A thin layer of garnet (*g*, bordering the quenched liquid) and low-Ca pyroxene (*op*) occurs along the upper part of the sample capsule (in contact with the thermocouple). (b) SEM-BSE image of enlarged portion near the upper capsule wall. The width of the image is 0.3 mm.

periment DC409, Fig. 3) garnet is the liquidus phase, followed at lower temperature by low-Ca pyroxene.

The quenched melt and liquidus phase compositions are listed in Table 1 together with the composition of the starting materials (AUK and ADK). The melt compositions are roughly similar to the bulk system compositions, with deviations resulting from the mineral-melt mass balance. The somewhat larger differences between the bulk system and the quenched melt composions in the two 'reversed' experiments are due to the crystallization of relatively large amounts of the liquidus phase (garnet in 1272 and olivine in 1276).

The olivines are generally characterized by the Mg/(Mg + Fe) ratio increasing as a function of increasing pressure and temperature. A significant pyroxene solid solution is present in the garnets, and the liquidus garnet at 8.5 GPa (AUK:1272) and 11 GPa (ADK:DC409) have mole fractions of Al-free pyroxene end members of 14% and 35%, respectively (100 − (Al + Cr) · 50 based on 12 oxygen atoms, Table 1).

3.3 Phase relations of C1 chondrite from 20 to 27 GPa

Table 2 presents the bulk system and liquidus mineral compositions of the experiments on average C1 chondrite in the system CaO-MgO-FeO-Al_2O_3-SiO_2. Magnesiowüstite/ferropericlase is present as an additional near-liquidus or liquidus phase over the entire 20–27 GPa pressure range [14]. The composition of this phase is extremely sensitive to the position of the analysed grain relative to the liquidus (increasing Fe/Mg ratio from the liquidus towards the solidus; see [14]),

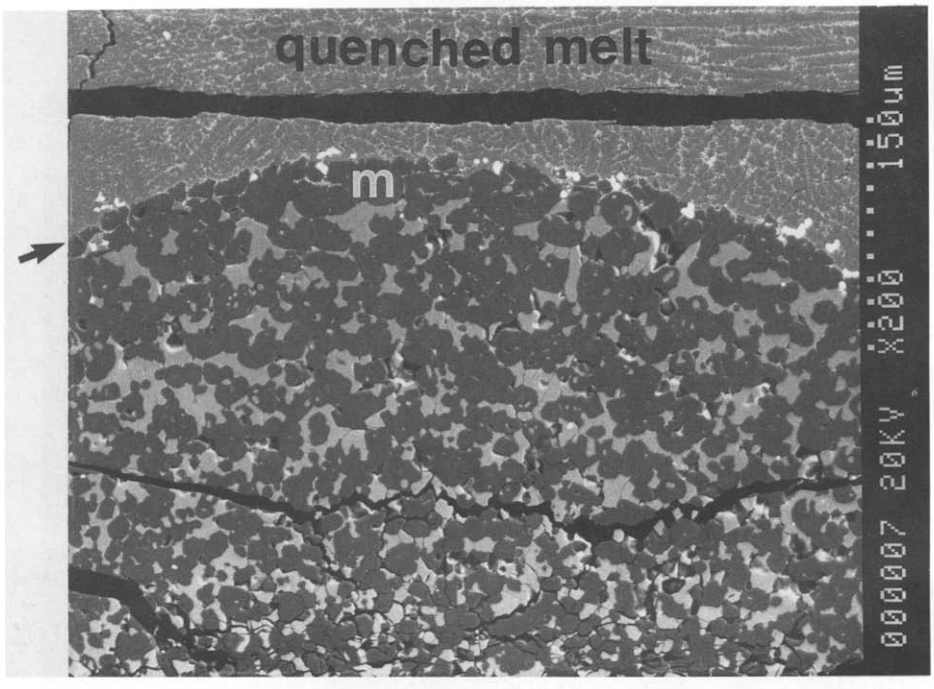

Fig. 4. SEM-BSE images of C1 chondrite run product 1273 at 25 GPa (Table 2). The long axis of the charge was oriented vertically during the experiment, with the melt above the solid part of the capsule. The width of the image is 0.5 mm, and the thermal gradient along the axis of the charge (vertical direction of the image, as well as during the experiment) is approximately 200°C/mm. The liquidus interphase (marked with an arrow in the left-hand margin of the image) is estimated to be the 2150°C isotherm. Majorite (*m*) appears to be the liquidus phase, and the other major phase below the liquidus is ferropericlase/magnesiowüstite (high BSE brightness, note increase in brightness and Fe/Mg ratio away from the liquidus). Small Re fragments (very bright) have sunk and settled on the liquidus interphase.

and will not be discussed further here. Figure 4 illustrates the liquidus phase relations of experiment 1273 (25 GPa). The Al-free pyroxene component ranges from 40% (20 GPa) to 52% (25 GPa) of the liquidus majorites and reaches 76% in the liquidus perovskite.

Attempts to analyze the quenched melt compositions resulted in high and variable Al contents because of the strong influence of quenched majorite relative to an interstitial Fe-Mg-rich phase (local surface polishing and textural effects). Based on the analyses and a semi-quantitative correction for the quenched majorite effect, the melt composition appears to be similar to the bulk system composition in all of the experiments, and the bulk system composition was therefore used to derive the partitioning coefficients.

4. mineral-melt partitioning

4.1 Introduction and data presentation

The Nernst mineral-melt distribution coefficient ($D_i = C_i^{\min}/C_i^{\text{melt}}$, where C_i is the concentration of element i) for major elements such as Fe and Mg varies widely as a function of melt composition and pressure. In contrast, the exchange distribution coefficient $K_D = (C_i/C_j)^{\min}/(C_i/C_j)^{\text{melt}}$ for the Fe/Mg ratio is remarkably independent of composition and temperature, because of the geochemical similarity of these two elements, and because the compositional effects on the D_i for Fe and Mg cancel out [21]. In their discussion of element partitioning between mantle minerals and melts, Hanson and Langmuir [22] classified the elments as trace elements, essential structural constituents (ESC: Si, Al, Ca) and intermediate elements (Fe, Mg). The ratios of true ESCs are constant for a given mineral, and the variation in exchange distribution coefficients for ESCs will therefore only reflect the variation in melt composition. The increasing solubility of pyroxene components in garnet at pressures above 5 GPa, however, implies that Si, Ca and Al are not strictly ESCs in the deeper portions of the upper mantle and in the transition zone. Regardless of the type element behaviour, the application of exchange distribution coefficients is a very useful and direct way of illustrating the variation of an element ratio as a result of melt-solid fractionation. Cr is the only 'trace element' discussed in this paper. Occurring in concentrations of up to 4800 and 8200 ppm (0.7 and 1.2 wt% Cr_2O_3) in komatiitic liquid and garnet respectively, it is uncertain whether Cr obeys Henry's law.

Because the main objective of this study is to evaluate the chemical consequences of melt-solid fractionation throughout the upper mantle, transition zone and uppermost lower mantle, we show the distribution coefficients for selected element ratios (Si/Mg, Fe/Mg, Ca/Al) and Cr at different pressures in Figs. 5–7. It is important to note, however, that the observed trends are also functions of temperature and composition (bulk system and melt composition). As a result of the increase in liquidus and solidus temperatures with increasing pressure [e.g. 15], the temperatures and pressures are in general positively correlated in the experimental data base used in this study (Tables 1 and 2 and [16–18,23–35]). In this compilation the liquidus temperature ranges from less than 1300°C for basalts at 1 GPa to 2000–2500°C for peridotites and chondrites at 20–27 GPa. The normative olivine contents of the melts (and of the bulk starting materials) are also in general positively correlated with both the pressure and temperature of the experiments.

In the discussion of the mineral-melt element partitioning we will not attempt to isolate the effects of temperature and melt composition from that of pressure. We note, however, that in the experimental studies that constitute our data base the starting material compositions, and therefore the liquidus temperature of the systems, are to a large extent chosen such that the bulk system is relevant to the expected melt-solid compositions within the investigated pressure ranges (1–3 GPa: basalt–peridotite; 4–10 GPa: komatiite–peridotite; 10–27 GPa: peridotite liquid–peridotite or peridotite liquid–majorite-perovskite dominated assemblages).

The considerable scatter in the data at a given pressure, especially in Fig. 7, is a result of several factors, including compositional and temperature variations, analytical errors and experimental errors (e.g. pressure and temperature uncertainties, and a largely unconstrained oxygen fugacity). The

uncertainties in Fig. 7 are to a large extent also of an interlaboratory nature.

The new partitioning data presented in Fig. 5 and Fig. 6 are consistent with the mineral-melt compositional data presented in the literature [16–18,23–35]. In the following discussion of the variation of each of the individual partition coefficients we will therefore refer to Fig. 6, which displays all the data.

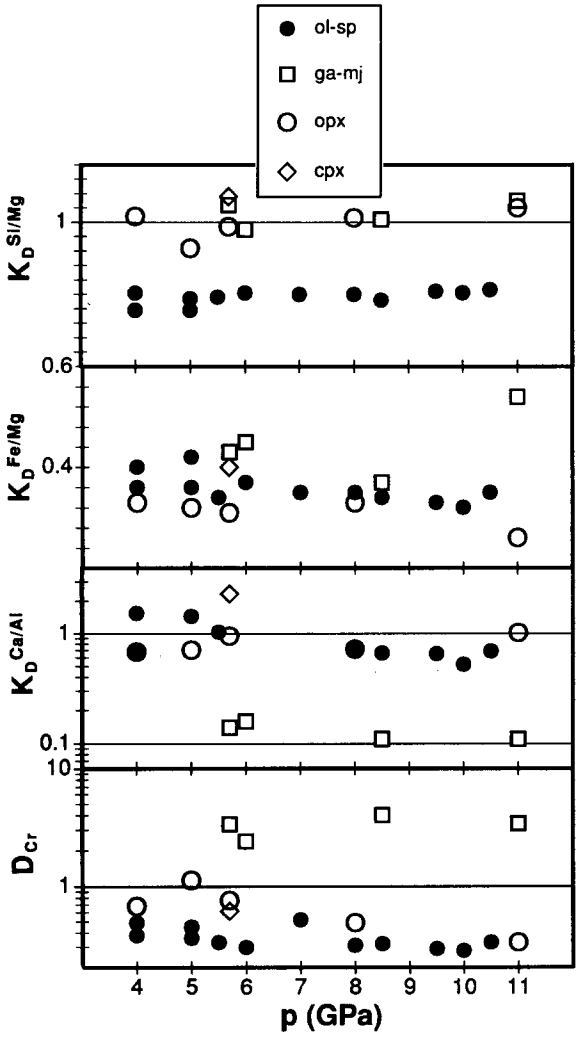

Fig. 5. The exchange distribution coefficient $K_D^{i/j} = (C_i/C_j)^{min}/(C_i/C_j)^{melt}$ for the ratios Si/Mg, Fe/Mg and Ca/Al, and the Nernst distribution coefficient $D_{Cr} = Cr^{mineral}/Cr^{melt}$ at different pressures for the komatiite experiments (Table 1). Mineral abbreviations in legend as in Fig 7.

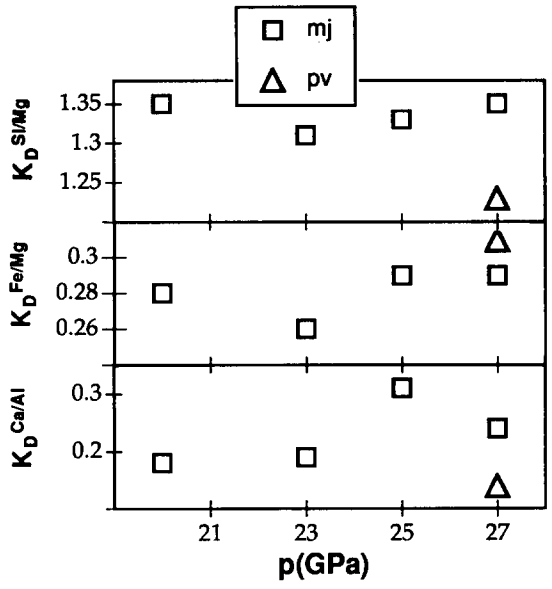

Fig. 6. mineral-melt distribution coefficients (as in Fig. 5) for the C1 chondrite experiments (Table 2). Mineral abbreviations in legend as in Fig 7.

4.2 *Si / Mg*

The $K_D^{Si/Mg}$ increases with increasing depth for all the mantle minerals (Fig. 7). Most of the increase is within the 30–180 km range. Because Si and Mg approximate ESC behaviour, the $K_D^{Si/Mg}$ variation will largely reflect the changing melt composition. Increasing liquidus stability of garnet/majorite at the expense of olivine at elevated pressure [e.g. 12,15] results in melts with higher normative olivine content, and if the mineral compositions are nearly constant, $K_D^{Si/Mg}$ is expected to increase as a function of pressure. Because the garnet $K_D^{Si/Mg}$ exceeds unity, extensive partial melting of a bimineralic peridotite (β-spinel and majorite) in the transition zone, where majorite is the liquidus (and the residual) phase, may produce a melt which is more magnesian than the source. Such a relationship may also persist into the lower mantle where Mg-Fe-silicate perovskite is likely to be the liquidus phase (Fig. 7).

4.3 *Fe / Mg*

The $K_D^{Fe/Mg}$ for olivine/β-spinel increases slightly from 0.3 at 1 GPa to almost 0.4 at 11 GPa

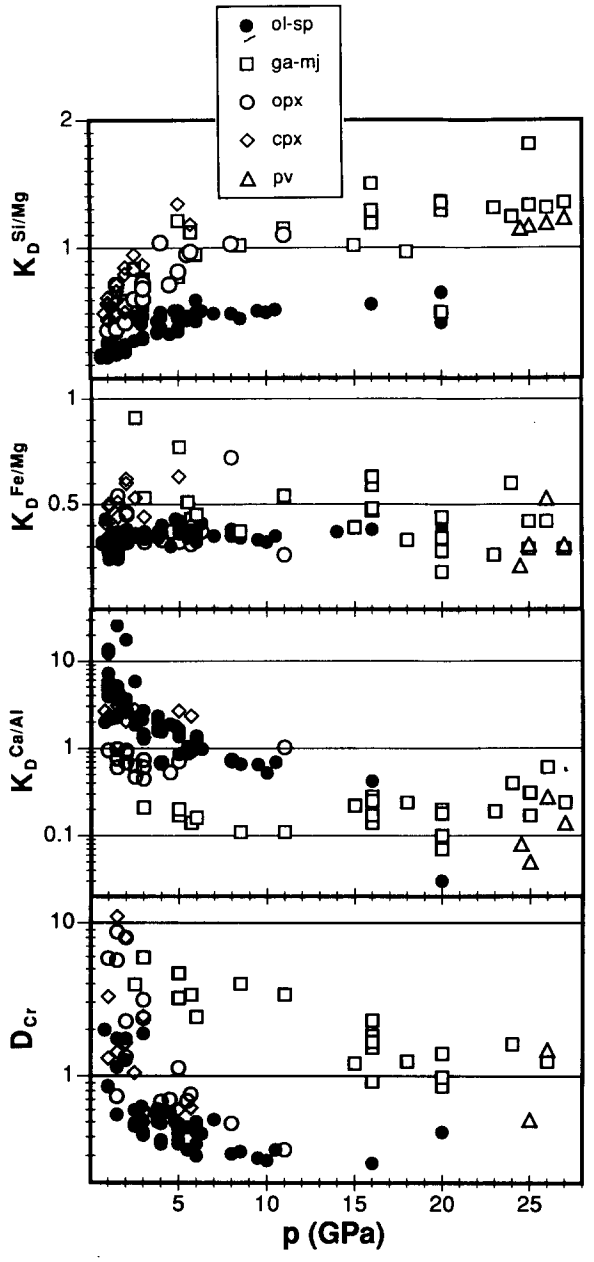

Fig. 7. mineral-melt distribution coefficients (as in Fig. 5) compiled from Tables 1 and 2 and [16–18,23–34]. Mineral abbreviations in legend: *ol–sp* = olivine and β-spinel; *ga–mj* = garnet and majorite; *opx* = low-Ca pyroxene; *cpx* = high-Ca pyroxene; *pv* = Mg-Fe-silicate perovskite.

and remains around 0.4 up to 20 GPa (Fig. 7). The increase in $K_D^{Fe/Mg}$ for orthopyroxene is nearly identical to that of olivine, whereas the increase for clinoproxene appears to be much more rapid (0.6 at 5 GPa). There is, however, considerably more scatter in the data for clinopyroxene and garnet/majorite. The variation trend for garnet/majorite is towards lower $K_D^{Fe/Mg}$ with increasing depth (about 0.4 near the 670 km discontinuity). Perovskite also has a low $K_D^{Fe/Mg}$, of 0.2–0.5. As pointed out by Takahashi [6], the experimentally derived $K_D^{Fe/Mg}$ values are likely to be higher rather than lower than the real partitioning values because of suspected preferential loss of Fe from the melt phase.

The derived $K_D^{Fe/Mg}$ for olivine/β-spinel in the 5–20 GPa range is considerably lower than the values obtained by a linear extrapolation of the 0–3 GPa variation reported by Ford et al. [3] and Ulmer [4]. At pressures less than the stability of residual magnesiowüstite, the chemical consequence of melt extraction is therefore a relatively uniform increase in the Mg# [= Mg/(Mg + Fe)] of mantle residues.

4.4 Ca/Al

The $K_D^{Ca/Al}$ for olivine and clinopyroxene decreases strongly from 5 (cpx) and 10–20 (ol) at 1 GPa to about 1 at 5–7 GPa, and the olivine/β-spinel value decrases further at higher pressures and temperatures (Fig. 7). Due to the low concentration of Ca and Al in olivine and β-spinel, however, the $K_D^{Ca/Al}$ uncertainties for these minerals are considerably larger than for the other phases. The orthopyroxene values are below unity in this range but appear to increase to almost 2 at 10–12 GPa. Garnet/majorite has an almost constant $K_D^{Ca/Al}$ of 0.1–0.3 throughout the 3–27 GPa range, and the perovskite values are similar or even lower.

Because spinel and garnet are minor consituents of the uppermost 100 km of the mantle, progressive melt extraction from this region may result in residues where the Ca/Al ratio stays constant or slightly increases as a function of melt fraction. At depths exceeding 150 km, however, garnet/majorite-bearing residues will be Al-enriched and the melts will be correspondingly Al-depleted.

4.5 Cr

D_{Cr} decreases with increasing depth: strongly for olivine/β-spinel, and the pyroxenes in the

30–150 km range, but only slightly for garnet/majorite throughout the entire upper mantle (Fig. 7). The values for basaltic and andesitic rocks listed by Henderson [9] are 2, 10 and 8 for olivine, orthopyroxene and clinopyroxene, respectively. These are similar to the 1–2 GPa range values based on the mineral and glass compositions of Bender et al. [24], Takahashi and Kushiro [25], and Elthon and Scarfe [26] (plotted in Fig. 6), whereas the olivine-melt values derived from Bickle et al. [23] and Agee and Walker [33] are below unity (0.4–0.6). Because the latter papers [23,33] provide compositions of more olivine-melt pairs than the former papers [24–26] (13 versus 8) in the 0.8–3.8 GPa range, the olivine trend in Fig. 6 is possibly somewhat biased towards lower values in this pressure range. Cr is most likely a strongly compatible element during melting and crystallization in the uppermost mantle (to depths of 100–150 km), especially when spinel and/or garnet are residual or cystallizing phases. The strong decrease in D_{Cr} for olivine/β-spinel and orthopyroxene (down to 0.3–0.5 at 10–20 GPa) and the moderate decrease for garnet (down to 1.2–1.6 at 10–26 GPa), however, will probably result in a bulk distribution coefficient for Cr near unity for assemblages containing both olivine/β-spinel and garnet/majorite in the 200–670 km depth range. If olivine/β-spinel is the only residual phase, Cr will be even more compatible.

5. Implications for mantle evolution

The various types of upper mantle peridotites (xenoliths, alpine-type peridotites, abyssal peridotites and ophiolites) have systematic chemical variations that are suggestive of varying degrees of partial melting and melt extraction [36–38]. Klein and Langmuir [10] and McKenzie and Bickle [39] have shown that the melting of adiabatically rising mantle is polybaric and that the depth of initial melting (intersection between the adiabatic path and the solidus in T–p space) is simply related to the mantle potential temperature. Because melt extraction will occur at low melt fractions [40], the melt accumulated at a shallow level (e.g. the Moho) will have a composition corresponding to the average of a range of melt compositions generated throughout the melting column. The potential mantle temperature varies geograpically along the systems of oceanic ridges, and is higher in areas influenced by mantle plumes [10]. The potential mantle temperature has presumably also decreased over time from a maximum soon after the formation of the core, or during maximum bombardment at a late accretionary stage, to a present low value.

The relatively constant Cr contents (3000 ppm) of upper mantle peridotites covering the entire 35–49% MgO range led Liang and Elthon [8] to conclude that the composition of upper mantle peridotites records a history of melt extraction during which the distribution coefficient of Cr was close to unity, and that the extracted melts were dominantly komatiitic and picritic. Our finding that Cr changes from a strongly compatible element to one with a bulk distribution coefficient near unity for garnet + olivine residues at a pressure of about 5 GPa supports their conclusions, and indicates that the time-integrated, and averaged, melt extraction from the mantle has been deep-seated komatiitic, rather than shallow and basaltic. The fact that harzburgitic residues from extensive melting at depths exceeding 150 km [e.g. 12,35] will be depleted in Cr relative to the original peridotite sources may also contribute to the observed Cr abundances in mantle peridotites. If some of the most fertile peridotites (less than about 38 wt% MgO) were metacumulates rather than weakly depleted residues after melt extraction, the constant Cr over the full range of peridotitic MgO contents could also in part be caused by Cr enrichment by crystallization of, for example, pyroxenes and spinel.

If a large part of the time-integrated melt extraction from the mantle occurred from depths exceeding 150 km, it was probably largely linked to Archean komatiitic magmatism. A considerable portion of the melt that ultimately (after shallow fractionation) produces the basaltic magmas injected into oceanic and continental crust, however, may be extracted as picritic or komatiitic batches from a depth of 100–200 km [8]. Storey et al. [41] also suggested that komatiites may be relatively common in Phanerozoic oceanic plateaus.

Because the bulk $K_D^{Fe/Mg}$ is uniformly low (0.3–0.5) throughout the 3–27 GPa pressure range, the Mg number of upper mantle peri-

dotites provides no information about the depth of melt extraction and the composition of the extracted melt. Rather, the Mg number will be a convenient and nearly pressure-independant measure of the degree of melt depletion.

Several different compositional models have been proposed for the bulk silicate Earth and for the primitive upper mantle [e.g. 7,42,43]. Most of these models are based on a comparison of the compositions of upper mantle lherzolites and chondrites, although Anderson [43] argued for the use of solar element abundances. Recent estimates of the solar system composition based on solar energetic particles [references in 43] differ considerably from the carbonaceous chondrite composition [e.g. 44], although the uncertainties are very large. Estimates of the terrestrial mantle composition based on solar, chondritic and actual lherzolitic element abundances have CaO/Al_2O_3 ratios of 1.06, 0.79 and 0.90, respectively. The solar compositional uncertainties, however, are so large that the solar value (the largest) may overlap even the chondritic value [43]. Both Ca and Al are highly refractory elements and should not be fractionated during the condensation and accretion processes. Therefore, *intraplanetary* fractionation is a very tempting explanation for the higher Ca/Al ratio of most of the upper mantle peridotites relative to the C1 carbonaceous chondrites, although Hart and Zindler [42] caution that the elevated Ca/Al of mantle xenoliths could result from a biased sampling of clinopyroxene-rich specimens.

Because the bulk $K_D^{Ca/Al}$ is lower than 1 for assemblages containing garnet or majorite, the residues are expected to aquire a lower Ca/Al ratio than the source. The extremely depleted low-temperature peridotite xenoliths from the Kaapvaal craton have lower than chondritic Ca/Al ratios, and Boyd [5] suggested that they are complementary to magmas similar to the 3.45 Ga old Al-depleted komatiites of the Barberton greenstone belt in the same area. If the extraction of somewhat Al-depleted magmas was a mantle-wide phenomenon, the upper mantle might have had an initial Ca/Al ratio even higher than the present prior to the melt depletion recorded by major and trace element variations. The possible failure of some Al-depleted komatiitic magmas to reach the surface, however, may contribute to the elevated Ca/Al ratio of the uppermost sampled part of the mantle relative to the chondritic ratio.

With the exception of the Kaapvaal low-temperature xenoliths, the Ca/Al ratio of upper mantle peridotites is generally not correlated with the degree of melt depletion (the latter being indicated by the total MgO content or the Mg number) [e.g. 5,15]. Assuming that much of the time-integrated melt depletion was in the form of deep-level komatiite extraction, it is likely that garnet or majorite was often totally consumed during melting. No major change would therefore be imposed on the Ca/Al ratio of melts and residues.

A small amount of majorite and/or perovskite fractionation from the upper mantle soon after the formation of the Earth is a simple process capable of increasing the Ca/Al ratio. A consistent difference between the cosmic abundances and the Earth's upper mantle is the higher SiO_2/MgO cosmic ratio (both solar and chondritic values of 1.4 versus 1.0 for average lherzolite). Although Ringwood [45] and Ringwood and Hibberson [46] have ascribed this difference to variable solar nebulae volatility and variable core solubility between the two elements, the discrepancy remains enigmatic. Because the $K_D^{Si/Mg}$ for both majorite and perovskite exceeds unity, an early fractionation of one or both of these phases from the upper mantle would increase its Mg/Si ratio relative to the transition zone and the lower mantle. This effect would possibly be reversed, however, if magnesiowüstite was part of the fractionating assemblage.

Major element models of the evolution of a chondritic magma ocean involving majorite fractionation [47] and perovskite fractionation combined with olivine accumulation [48] have successfully derived upper mantle peridotite compositions. The trace element behaviour during these processes is uncertain [28–30,48], and it is difficult to test the models rigorously. If the 3.45 Ga old Al-depleted komatiites of the Barberton greenstone belt were formed from a majorite-depleted mantle reservoir produced during the crystallization of a magma ocean 4.6–4.4 Ga ago, the expected $\epsilon(3.45)_{Hf}$ value would be within the -8 to -6 range [49]. The $\epsilon(3.45)_{Hf}$ values measured by Gruau et al. [49], however, are very close

to zero, indicating that the garnet/majorite fractionation required to produce these Al-depleted melts occurred *during* the magmatic event.

6. Conclusions

(1) The bulk mantle–melt distribution coefficient of Cr decreases towards unity at depths exceeding 100–150 km for residues including olivine/β-spinel, pyroxenes and garnet/majorite, and will be below unity for harzburgitic and dunitic residues. At shallow mantle levels (pressures below 3 GPa) Cr is a strongly compatible element and melt extraction will produce Cr-enriched residues. Upper mantle peridotites, however, have nearly constant Cr contents over the entire range of MgO contents [8]. A large proportion of the time-integrated melt extraction from the mantle was komatiitic, and the average depth of melt separation was greater than 100 km. The proportion of komatiite relative to picrite and basalt extraction can be reduced if a large proportion of the komatiitic magmatism involved extensive melting and deep-level melt separation from harzburgitic residues [12,35].

(2) The $K_D^{Fe/Mg}$ for olivine/β-spinel, pyroxenes, garnet/majorite and perovskite remains low (0.3–0.5) throughout the upper mantle, the transition zone and the uppermost lower mantle, and the Mg number of peridotites is therefore a depth-independant indicator of melt depletion.

(3) The Ca/Al ratio of depleted mantle peridotites would decrease considerably by high-pressure (> 5 GPa) melt extraction leaving behind garnet/majorite-bearing residues. This appears to be in conflict with the higher than chondritic Ca/Al ratio in most mantle peridotites (with the exception of the strongly depleted low-temperature peridotites from the Kaapvaal craton [5]) but is consistent with the suggestion that most of the deep-level komatiite extraction was in the form of Al-undepleted melts separated from harzburgitic residues [12,35]. The elevated Ca/Al ratio of sampled mantle peridotites relative to chondrites can partly be ascribed to Al-depleted komatiite addition to the uppermost mantle. Minor garnet and/or perovskite fractionation from an early magma ocean may also contribute to the high Ca/Al ratio.

(4) The $K_D^{Si/Mg}$ for majorite and perovskite exceeds unity. Melting or fractionation of a relatively fertile peridotite composition in the transition zone and the uppermost lower mantle would therefore produce a melt with a Si/Mg ratio that is lower than that of the source.

Acknowledgements

We thank the technical staff supporting the multi-anvil laboratories in Edmonton and Bayreuth, Paul Wagner (microanalysis, University of Alberta) and Christine Payette (BSE imaging, CANMET). This research was supported by a postdoctoral fellowship (D.C.), an operating grant (R.G.T.) and major installation and infrastructure grants (C.M. Scarfe and R.W. Luth) from the Natural Sciences and Engineering Research Council of Canada. Claude Herzberg supplied preprints [12,47], and the three journal reviewers provided useful critisism.

References

1 G. Wetherill, Formation of the Earth, Annu. Rev. Earth. Planet. Sci. 18, 205–256, 1990.
2 P.L. Roeder and R.F. Emslie, olivine-liquid equilibrium, Contrib. Mineral. Petrol. 29, 275–289, 1970.
3 C.E. Ford, D.G. Russell, J.A. Craven and M.R. Fisk, olivine-liquid equilibria: temperature, pressure and composition dependance on the crystal/liquid partitioning coefficient for Mg, Fe^{2+}, Ca and Mn, J. Petrol. 24, 256–265, 1983.
4 P. Ulmer, The dependance of the Fe^{2+}-Mg cation partitioning between olivine and basaltic liquid on pressure, temperature and composition. An experimental study to 30 kbars, Contrib. Mineral. Petrol. 101, 261–273, 1989.
5 F.R. Boyd, Compositional distinction between oceanic and cratonic lithosphere, Earth Planet. Sci. Lett. 96, 15–26, 1989.
6 E. Takahashi, Speculations on the Archean mantle: missing link between komatiite and depleted garnet peridotite, J. Geophys. Res. 95 (B10), 15945–15954, 1990.
7 H. Palme and K.G. Nickel, Ca/Al ratio and composition of the Earth's upper mantle, Geochim. Cosmochim. Acta 49, 2123–2132, 1985.
8 Y. Liang and D. Elthon, Evidence from chromium abundances in mantle rocks for extraction of picrite and komatiite melts, Nature 343, 551–553, 1990.
9 P. Hendersson, Inorganic Geochemistry, Pergamon, Oxford, 1982.
10 E.M. Klein and C.H. Langmuir, Global correlation of ocean ridge basalt chemistry with axial depth and crustal thickness, J. Geophys. Res. 92 (B8), 8089–8115, 1987.
11 V.M.J. Salters and S.R Hart, The hafnium paradox and the role of garnet in the source of mid-ocean-ridge basalts, Nature 342, 420–422, 1989.

12 C. Herzberg, Depth and degree of melting of komatiites, J. Geophys. Res. 97, in press, 1992.
13 K. Wei, R.G. Trønnes and C.M. Scarfe, Phase relations of aluminum-undepleted and aluminum-depleted komatiites at pressures of 4–12 GPa, J. Geophys. Res. 95 (B10), 15817–15827, 1990.
14 R. Trønnes, Liquidus phase relations of C1 chondrite at pressures of 20–27 GPa, Eos Trans. Am. Geophys. Union 73, 317, 1992.
15 C. Herzberg, T.Gasparik and H. Sawamoto, Origin of mantle peridotite: Constraints from experiments to 16.5 GPa, J. Geophys. Res. 95 (B10), 15799–15803, 1990.
16 E. Takahashi, Melting of a dry peridotite KLB-1 up to 14 GPa: implications for the origin of peridotitic upper manlte, J. Geophys. Res. 91 (B8), 9367–9382, 1986.
17 E. Ito and E. Takahashi, Melting of peridotite at uppermost lower mantle conditions, Nature 328, 514–517, 1987.
18 E. Ohtani and H. Sawamoto, Melting experiment on a model chondritic mantle composition at 25 GPa, Geophys. Res. Lett. 14, 733–736, 1987.
19 T. Gasparik, Transformation of enstatite-diopside-jadeite pyroxenes to garnet, Contrib. Mineral. Petrol. 102, 389–405, 1989.
20 E. Ito and E. Takahashi, Postspinel transformations in the system Mg_2SiO_4-Fe_2SiO_4 and some geophysical implications, J. Geophys. Res. 94 (B8), 10637–10646, 1989.
21 P.L. Roeder, Activity of iron and olivine solubility in basaltic liquids, Earth Planet. Sci. Lett. 23, 397–410, 1974.
22 G.N. Hanson and C.H. Langmuir, Modelling of major elements in mantle-melt systems using trace element approaches, Geochim. Cosmochim. Acta 42, 725–741, 1978.
23 M.J. Bickle, C.E. Ford and E.G. Nisbet, The petrogenesis of peridotitic komatiites: evidence from high-pressure melting experiments, Earth. Planet. Sci. Lett. 37, 97–106, 1977.
24 J.F. Bender, F.N Hodges and A.E. Bence, Petrogenesis of basalts from the project FAMOUS area: experimental study from 0 to 15 kbars, Earth. Planet. Sci. Lett. 41, 277–302, 1978.
25 E. Takahashi and I. Kushiro, Melting of a dry peridotite at high pressures and basalt magma genesis, Am. Mineral. 68, 859–879, 1983.
26 D. Elthon and C.M. Scarfe, High-pressure phase equilibria of a high-magnesia basalt and the genesis of primary oceanic basalts, Am. Mineral. 69, 1–15, 1984.
27 E. Ohtani, T. Kato and H. Sawamoto, Melting of a model chondritic mantle to 20 GPa, Nature 322, 352–353, 1987.
28 T. Kato, T. Irifune and A.E. Ringwood, Majorite partition behavior and petrogenesis of the Earth's upper mantle, Geophys. Res. Lett. 14, 546–549, 1987.
29 T. Kato, A.E. Ringwood and T. Irifune, Experimental determination of element partitioning between silicate perovskites, garnets and liquids: constraints on early differentiation of the mantle, Earth. Planet. Sci. Lett. 89, 123–145, 1988.
30 T. Kato, A.E. Ringwood and T. Irifune, Constraints on element partitioning coefficients between $MgSiO_3$ perovskite and liquid by direct determination, Earth. Planet. Sci. Lett. 90, 65–68, 1988.
31 E. Ohtani, I. Kawabe, J. Moriyama and Y. Nagata, Partitioning of elements between majorite garnet and melt and implications for the petrogenesis of komatiites, Contrib. Mineral. Petrol. 103, 263–269, 1989.
32 C.B. Agee, A new look at differentiation of the Earth from melting experiments on the Allende meteorite, Nature 346, 834–837, 1990.
33 C.B. Agee and D. Walker, Aluminum partitioning between olivine and ultrabasic silicate liquid to 6 GPa, Contrib. Mineral. Petrol. 105, 243–254, 1990.
34 H. Yurimoto and E. Ohtani, Element partitioning between majorite and liquid: a secondary ion mass spectometric study, Geophys. Res. Lett. 19, 17–20, 1992.
35 D. Canil, Orthopyroxene stability along the peridotite solidus and the origin of cratonic lithosphere beneath southern Africa, Earth Planet. Sci. Lett. 111, in press, 1992.
36 F.A. Frey and M. Prinz, Ultramafic inclusions from San Carlos, Arizona: petrological and geochemical data bearing on their petrogenesis, Earth Planet. Sci. Lett. 38, 129–176, 1978.
37 F.A. Frey, C.J. Suen and H.W. Stockman, The Ronda high temperature peridotite: geochemistry and petrogenesis, Geochim. Cosmochim. Acta 49, 2469–2491, 1985.
38 K.T.M. Johnson, H.J.B. Dick and N. Shimizu, Melting in the oceanic upper mantle: an ion microprobe study of diopsides in abyssal peridotites, J. Geophys. Res. 95 (B3), 2661–2678, 1990.
39 D. McKenzie and M.J. Bickle, The volume and composition of melt generated by extension of the lithosphere, J. Petrol. 29, 625–679, 1988.
40 D. McKenzie, The generation and compaction of partially molten rock, J. Petrol. 25, 713–765, 1984.
41 M. Storey, J.J. Mahoney, L.W. Kroenke and A.D. Saunders, Are oceanic plateaus sites of komatiite formation?, Geology 19, 376–379, 1991.
42 S.R. Hart and A. Zindler, In search of a bulk-Earth composition. Chem. Geol. 57, 247–267, 1986.
43 D.L. Anderson, Composition of the Earth, Science 243, 376–370, 1989.
44 E. Anders and N. Grevesse, Abundances of the elements: meteoritic and solar, Geochim. Cosmochim. Acta 53, 197–214, 1989.
45 A.E. Ringwood, Significance of the terrestrial Mg/Si ratio, Earth Planet. Sci. Lett. 95, 1–7, 1989.
46 A.E. Ringwood and W. Hibberson, Solubilities of mantle oxides in molten iron at high pressures and temperatures: implications for the composition and formation of the Earth's core, Earth Planet. Sci. Lett. 102, 235–251, 1991.
47 C. Herzberg and T. Gasparik, Garnet and pyroxenes in the mantle: a test of the majorite fractionation hypothesis, J. Geophys. Res. 96, 16263–16274, 1991.
48 C.B. Agee and D. Walker, Mass balance and phase density constraints on the early differentiation of chondritic mantle, Earth Planet. Sci. Lett. 90, 144–156, 1988.
49 G. Gruau, C. Chauvel, N.T. Arndt and J. Cornichet, Aluminum depletion in komatiites and garnet fractionation in the early Archean mantle: hafnium isotopic constraints, Geochim. Cosmochim. Acta 54, 3095–3101, 1990.